Numerical analysis of keyhole welding of mild steel plate with the plasma arc†

TASHIRO Shinichi*, MIYATA Minoru, TANAKA Manabu***, SHIN Kenei**** and TAKAHASHI Kuniaki******

Abstract

As an action to an environmental problem, car companies attempt to reduce the weight of a car body maintaining strength by adopting a tailored blank which joins different thick metal plates. Keyhole welding with the plasma arc is generally used for the tailored blank, because this process enables high speed welding suppressing thermal distortions. A weld defect such as an undercut occurs if a welding current is higher in order to increase the welding speed, since the arc pressure is enhanced due to an increase in plasma jet velocity. The numerical analysis of the plasma arc is able to assist in overcoming such a phenomenon. The analyses have been conducted by many researchers in order to understand the mechanism of keyhole welding with the plasma arc and design the suitable plasma torch. In this study, we have built a unified model considering the convection flow in the weld pool to study phenomena in the plasma and the weld pool. A keyhole diameter calculated by the pressure balance on the keyhole surface was compared with an experiment result. As a result, the keyhole diameter obtained from the simulation approximately agreed with that of the experiment and the reliability of the simulation result was confirmed.

KEY WORDS: (Simulation), (Plasma arc), (Keyhole)

1. Introduction

PAW (Plasma Arc Welding) is one of the welding processes employing non-consumable electrode such as GTAW (Gas Tungsten Arc Welding). The difference of GTAW and PAW is mainly torch geometry. The plasma arc torch has a water-cooled copper nozzle in front of the cathode to constrict the arc plasma the through thermal pinch effect[1]. So an arc plasma with high energy density and high arc pressure can be produced. PAW can realize high speed welding, deeper weld penetration and, furthermore, smaller thermal distortion. For these reasons PAW is employed for keyhole welding[2].

As an action to an environmental problem, car companies attempt to reduce the weight of the car body maintaining the strength by adopting a tailored blank which joins different thick metal plates[3]. Keyhole welding with a laser or the plasma arc is generally used for the tailored blank, because these processes enable high speed welding suppressing thermal distortions. Although the laser welding is superior to PAW in welding speed, it requires high investment for equipment. Therefore, PAW is attractive for economic reasons.

A weld defect such as an undercut occurs if a welding current is higher in order to increase the welding speed, since the arc pressure is enhanced due to an increase in plasma jet velocity. The numerical analysis of the plasma arc is able to assist in overcoming such a phenomenon. The analyses have been conducted by many researchers in order to understand the mechanism of keyhole welding with the plasma arc and to design a suitable plasma torch.

The numerical model of keyhole welding by the plasma arc considering only the base metal[4] and the model dealing with the cathode, the nozzles, the plasma and the base metal totally except for the convection flow of the weld pool[5] were reported. In this study, we have built a unified model also considering the convection flow in the weld pool and study phenomena in the plasma and the weld pool. Furthermore, a keyhole diameter calculated by the pressure balance on the keyhole surface was compared with an experiment result.

† Received on June 11, 2010
* Assistant professor
** Graduate school student
*** Professor
**** Fuji Heavy Industries Ltd

Transactions of JWRI is published by Joining and Welding Research Institute, Osaka University, Ibaraki, Osaka 567-0047, Japan

2. Simulation model

Figure 1 shows a schematic illustration of the calculation region. The size of the calculation region is 100 × 30mm. The calculation region consists of a tungsten cathode with the diameter of 3.2mm and the tip angle of 60 degrees, a water-cooled copper nozzle with the inner diameter of 3.2mm, the arc plasma, a base metal 1 and a base metal 2. The base metal 1 is mild steel with thickness of 1mm. The mild steel is usually used as a material of the car body. The base metal 2 is water-cooled copper with a thickness of 25mm. It is described in a frame of cylindrical coordinates with axial symmetry around the arc axis. The electrode gap is set to be 5mm. A direct arc current of 90A is given inside the cathode on the top boundary. As boundary conditions, the outside of the base metal 1 and the bottom of base metal 2 are set to be 0V. The other boundary conditions are the same as those in the literatures[6,7]. The shielding gases are introduced from the inner nozzle on the upper boundary at the flow rate of 0.8 L/min and from the outer nozzle at the flow rate of 10 L/min. Laminar flow is assumed, and the arc plasma is considered to be in local thermodynamic equilibrium (LTE). The other numerical modeling methods are given in detail in our previous papers[6,7]. The differential equations (1)-(6) are solved iteratively by the SIMPLER numerical procedure[8].

Mass continuity equation

$$\frac{1}{r}\frac{\partial}{\partial r}\left(r\rho v_r\right)+\frac{\partial}{\partial z}\left(\rho v_z\right)=0 \tag{1}$$

Radial momentum conservation equation

$$\begin{aligned}&\frac{1}{r}\frac{\partial}{\partial r}\left(r\rho v_r^2\right)+\frac{\partial}{\partial z}\left(\rho v_r v_z\right)=-\frac{\partial P}{\partial r}-j_z B_\theta\\&+\frac{1}{r}\frac{\partial}{\partial r}\left(2r\eta\frac{\partial v_r}{\partial r}\right)+\frac{\partial}{\partial z}\left(\eta\frac{\partial v_r}{\partial z}+\eta\frac{\partial v_z}{\partial r}\right)-2\eta\frac{v_r}{r^2}\end{aligned} \tag{2}$$

Axial momentum conservation equation

$$\begin{aligned}&\frac{1}{r}\frac{\partial}{\partial r}\left(r\rho v_r v_z\right)+\frac{\partial}{\partial z}\left(\rho v_z^2\right)=-\frac{\partial P}{\partial z}+j_r B_\theta\\&+\frac{\partial}{\partial z}\left(2\eta\frac{\partial v_z}{\partial z}\right)+\frac{1}{r}\frac{\partial}{\partial r}\left(r\eta\frac{\partial v_r}{\partial z}+r\eta\frac{\partial v_z}{\partial r}\right)+\rho g\end{aligned} \tag{3}$$

Energy conservation equation

$$\begin{aligned}&\frac{1}{r}\frac{\partial}{\partial r}\left(r\rho v_r h\right)+\frac{\partial}{\partial z}\left(\rho v_z h\right)=\frac{1}{r}\frac{\partial}{\partial r}\left(\frac{r\kappa}{c_p}\frac{\partial h}{\partial r}\right)\\&+\frac{\partial}{\partial z}\left(\frac{\kappa}{c_p}\frac{\partial h}{\partial z}\right)+j_r E_r+j_z E_z-R\end{aligned} \tag{4}$$

Current continuity equation

$$\frac{1}{r}\frac{\partial}{\partial r}\left(rj_r\right)+\frac{\partial}{\partial z}\left(j_z\right)=0 \tag{5}$$

Ohm's law

$$j_r=-\sigma E_r,\ j_z=-\sigma E_z \tag{6}$$

In the above equations, t [s] is time, h [J/kg] is enthalpy, P [Pa] is pressure, v_z [m/s] and v_r [m/s] are the axial and radial velocities, j_z [A/m^2] and j_r [A/m^2] are the axial and radial components of current density, g [m/s^2] is acceleration due to gravity, κ [W/m/K] is thermal conductivity, C_p [J/kg/K] is specific heat, ρ[kg/m^3] is mass density, η[Pa s] is viscosity, σ[A/V/m] is electrical conductivity, R [W/m^3] is radiation emission coefficient, E_r [V/m] and E_z [V/m] are the radial and axial components of the electric field defined by $E_r=-\partial V/\partial r$ and $E_z=-\partial V/\partial z$, where V [V] is electric potential. The azimuthal magnetic field B_θ [T] induced by arc current is evaluated by the following Maxwell's equation (7):

$$\frac{1}{r}\frac{\partial}{\partial r}\left(rB_\theta\right)=\mu_0 j_z \tag{7}$$

where, μ_0 [H/m] is permeability in vacuum. In order to solve the above equations (1) to (6), the special condition about thermal flux that occurs only at the electrode surface must be considered. An additional energy flux term at the cathode surface is needed in equation (4) considering thermionic cooling due to the emission of electrons, ion heating, and radiation cooling. The additional energy flux for the cathode H_k [W/m^2] is defined as equation (8):

$$H_K=-\varepsilon\alpha T^4-\left|j_e\right|\phi_K+\left|j_i\right|V_i \tag{8}$$

where, ε[-] is surface emissivity, α[W/m^2/K^4] is the Stefan-Boltzmann constant, φ_K [V] is the work function of the tungsten cathode, V_i [V] is the ionization potential of argon, j_e [A/m^2] is electron current density, and j_i [A/m^2] is ion current density. As to thermionic emission of electrons at the cathode surface, j_e cannot exceed the Richardson current density J_R [A/m^2] [9] given by equation (9):

$$\left|j_R\right|=AT^2\exp\left(-\frac{e\phi_{Ke}}{k_B T}\right) \tag{9}$$

where, A [A/m^2/K^2] is the thermionic emission constant for the cathode surface, φ_e [V] is the effective work function for thermionic emission of the electrode surface at the local surface temperature, and k_B [J/K] is

the Boltzmann's constant. The ion-current density j_i is then assumed to be $|j|-|j_R|$ if $|j|$ is greater than$|\ |j_R|$, where $|j|=|j_e|+|j_i|$ is total current density at the cathode surface obtained from equation (5) Similarly, for the anode surface, equation (4) needs an additional energy flux term for heating by electron condensation (thermionic heating) and radiation cooling. The additional energy flux for the anode H_A [W/m^2] is defined as equation (10):

$$H_A = -\varepsilon\alpha T^4 + |j|\phi_A \tag{10}$$

where, φ_A [V] is the work function of the anode and $|j|$ is current density at the anode surface obtained from equation (5). The term including φ_A accounts for heating of the anode by electrons, which delivers energy equal to the work function absorbed at the anode. This term is analogous to the cooling effect that occurs at the cathode when electrons are emitted.

In this study, calculations are conducted in cases of keyhole diameters of 2.0mm, 2.5mm and 3.0mm. A possible keyhole diameter in this calculation condition is estimated by pressure balance on the keyhole surface. **Figure 2** shows a schematic illustration of the pressure balance on the keyhole surface. The surface tension of the weld pool acts as the force decreasing the keyhole diameter. It is calculated by the equation (11).

$$P = y / R_k \tag{11}$$

Where y [N/m] is surface tension and R_k [m] is keyhole radius. Because the surface temperature of the weld pool near the keyhole is very high, a large amount of metal vapor is generated. So the effect of metal vapor pressure cannot be ignored. Metal vapor pressure is calculated by equation (12) and (13)[10].

$$\log P_{Fe} = -19710/T - 1.27\log T + 13.27 \tag{12}$$

$$\log P_{Mn} = -14520/T - 3.02\log T + 19.24 \tag{13}$$

The shear force by the plasma jet influences the keyhole surface as expressed by the equation (14).

$$P = \eta \times V_z / dr \tag{14}$$

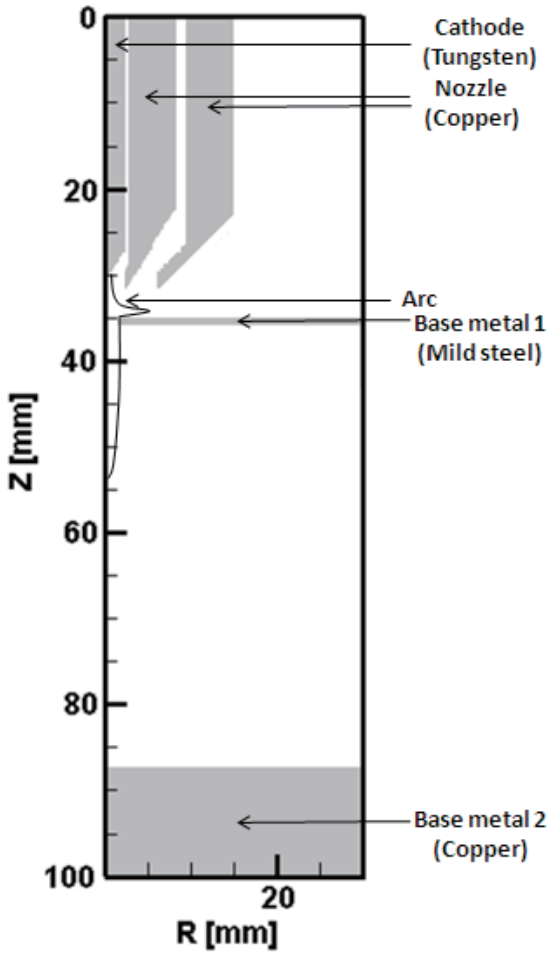

Fig. 1 Schematic illustration of calculation region.

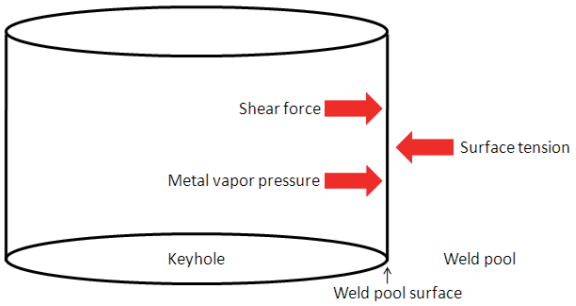

Fig. 2 Schematic illustration of pressure balances on keyhole surface.

3. Results and discussion

Figure 3 shows the temperature distribution of PAW in case when the keyhole diameter is 2.5mm.The maximum plasma temperature reached 21000K, and the maximum plasma jet velocity is 280m/sec. The base metal is covered with the plasma. It can be seen that the surface of the base metal near the keyhole is melted by the heat input from the arc. The heat in the weld pool is

transported outward in a radial direction and downward in an axial direction due to the convection flows in the weld pool generated by Marangoni forces and shear force by the plasma jet. So only the surface of the base metal is melted. Furthermore, the surface temperature of the weld pool near the keyhole is approximately 2000K uniformly. It is considered that a large amount of the metal vapor is generated on the surface and, consequently, the metal vapor and the plasma jet expand the keyhole.

Figure 4 shows the pressure balances at the surface of a keyhole. Average surface temperatures of the keyhole are 1990K, 2000K and 1940K in the cases of keyhole diameters of 2.0mm, 2.5mm and 3.0mm, respectively. The surface tension is 750 Pa when the keyhole diameter is 2.0mm. It was found that the surface tension decreases with increase in the keyhole diameter. Although the metal vapor pressure reaches 643 Pa when the keyhole diameter is 2.0mm, the metal vapor generated on the keyhole surface and its pressure decreases as the keyhole diameter increases because the surface temperature becomes lower. As with the metal vapor, the shear force by the plasma jet also decreases with increase in keyhole diameter. This is because the axial plasma jet velocity near the keyhole surface becomes slower. If the keyhole diameter is large, the keyhole is shrunk because the surface tension is larger than the metal vapor pressure and the shear force. On the other hand, if the keyhole diameter is small, the keyhole is expanded by the metal vapor pressure and the shear force. When the keyhole diameter is 2.3mm, the surface tension becomes the same as a total of the metal vapor pressure and the shear force. Because the pressures are balanced then, the keyhole is formed stably in this condition.

In this study, we also conducted an experiment in order to confirm the reliability of the simulation result. **Figure 5** shows an experimental setup consisting of a DC power source, a plasma torch, a base metal, a mirror and a video camera. The tungsten cathode has the diameter of 3.2mm and the tip angle of 60 degrees. A water-cooled copper nozzle with the inner diameter of 3.2mm was attached outside the cathode. The composition of a base metal is mild steel and the thickness is 1mm. The electrode gap is set to be 5mm. An arc current is set to be DC 90A and the shielding gas is argon. The flow rates of the shielding gas introduced from the inner nozzle and from the outer nozzle are 0.8 L/min and 10 L/min, respectively. **Figure 6** is a photograph of a keyhole captured from below the base metal through the mirror with the video camera. L3 and L4 are the keyhole diameters in the welding direction and transverse direction, respectively. It was found that L3 is 2.6mm and L4 is 2.2mm. As a result, the keyhole diameter obtained from the simulation approximately agrees with those of the experiment and the reliability of the simulation result was confirmed.

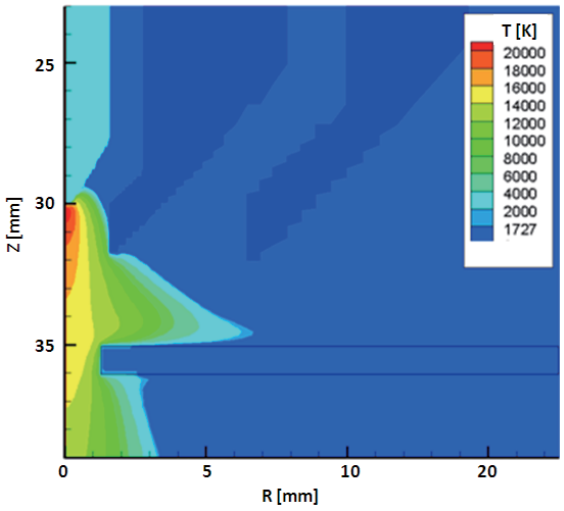

Fig. 3 Temperature distribution.

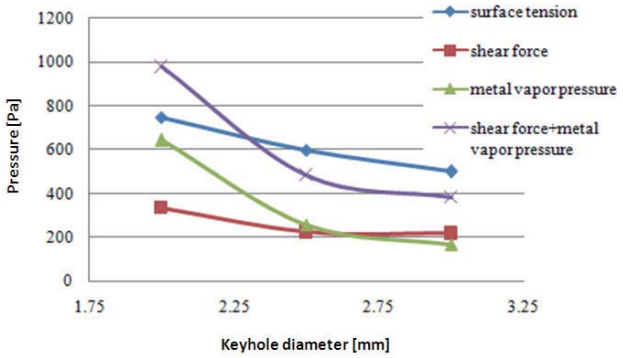

Fig. 4 Dependences of pressure balances on keyhole surface on keyhole diameter.

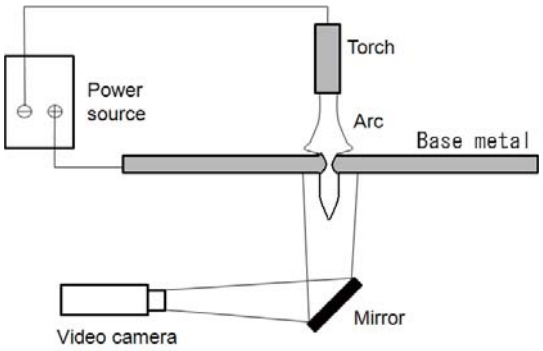

Fig. 5 Schematic illustration of experimental apparatus.

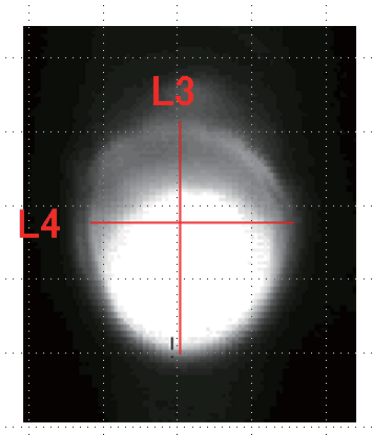

Fig. 6 Photograph of keyhole recorded with video camera.

4. Conclusions

In this paper, basic characteristic of plasma arc welding was examined. The main conclusions are summarized as follows.

(1) In PAW, plasma velocity and plasma temperature increase due to the thermal pinch effect.
(2) The heat in the weld pool is transported outward in a radial direction and downward in an axial direction due to the convection flows in the weld pool generated by Marangoni force and shear force of the plasma jet.
(3) The surface temperature of the weld pool near the keyhole is approximately 2000K uniformly.
(4) If the keyhole diameter is large, the keyhole shrinks because the surface tension exceeds the metal vapor pressure and the shear force. On the other hand, if the keyhole diameter is small, the keyhole is expanded by the metal vapor pressure and the shear force.
(5) The keyhole diameter obtained from the simulation approximately agrees with that of the experiment and the reliability of the simulation result is confirmed.

References

1) Tanaka M, Tashiro S, Satoh T, Murphy A B, Lowke J J; Sci.& Tech. Welding & Joining, 2008; 13: p.225.
2) Ali A H, Mori S, Fujii N, Yasuda K; Quarterly Journal of the Japan Welding Society, 2005; 23: p.245.
3) Uchihara M, Fukui K; Quarterly Journal of the Japan Welding Society, 2005; 23: p.549.
4) Fan H G, Kovacevic R; J. Phys. D: Appl. Phys, 1999; 32: p.2902.
5) Schnick M, Fussel U; IIW. doc. SG-212-1127-08.
6) Ushio M, Tanaka M, Lowke J J; IEEE Trans. Plasma Sci., 2004; 32: p.108.
7) Tanaka M et al; Metal. Trans. A, 2002; 33A: p.2043.
8) Patanker SV; Numerical Heat Transfer and Fluid Flow, Hemisphere Publishing Corporation, 1980.
9) Pfender E; Gaseous Electronics, Academic Press, 1978.
10) The Japan institute metals, edition no.3 data book of metals, Maruzen Co. Ltd., 1993 (in Japanese)